Graphic Visualization of Deformed Fibre-Reinforced Materials

V. M. Akhundov

Doctor of Physical and Mathematical Sciences,
National Metallurgical Academy of Ukraine, Ukraine

M. M. Kostrova

Post-graduate student
National Metallurgical Academy of Ukraine, Ukraine

I. Ju. Naumova

Candidate of Physical and Mathematical Sciences,
National Metallurgical Academy of Ukraine, Ukraine

Abstract
The current study reports on the visualization methodology applied for the units which represent the media of fibre-reinforced materials under conditions of large deformations. The units are visualized by the numerical solutions of the boundary problem, which shows the load on the materials in the deformed media. 3-D images of the deformed materials configurations are given with their unidirectional, bidirectional and three-directional schemes of reinforcement. These configurations are calculated with two level Akhundov's carcass theory employed for a piece of a homogeneous body.
Key words: FIBRE MATERIAL, UNIDIRECTIONAL REINFORCEMENT, TWO-WAY FIBRE REINFORCEMENT, TRI-ORTHOGONAL FIBRE REINFORCEMENT

Introduction

Visualization for fibre-reinforced materials under deformation is becoming topical. The past years have seen the various solutions for the mechanics of fibre-reinforced medium under large deformations and they are grounded on the approach of inner fields determination. A numerical solution of the deformation problem for the fibre-reinforced structure is able to define the inner fields in this kind of material and does it in the discrete forms determing inner fields

as the amounts of nodal points displacements within the constituents of a considered structure, deformational nodal values and stresses. The inner fields data are quite challenging for analysis even within the unit of the particular material, and it becomes more challenging to analyze the material behaviour of deformation and that of strength under large deformation in case if the material structure is more complex.

This problem is significantly easier to solve by means of numerical visualizations of a material initial configuration and a deformed one, the both are singled out from the medium of a fibre-reinforced material unit. Moreover, the external configuration of the deformed unit is its integral manifestation of the inner field. Therefore, applying visualizations of the material initial and deformed configurations one can forecast nodal points, in vicinity of which the material destruction can occur. Furthermore, the vicinity area belongs to a certain matrix, fibre, matrix-fibre boundary or interfacial layer and the information of its local state can be extracted in the run-time mode from the numerical solution performed for the mechanical task. Eventually, this information can undergo the additional processing and give solid-state report data.

However, the fibre-reinforced materials require more deep study from the standpoint of two-level analysis of its deformation. This is explained by the internal stability failure on both the material structure level (meso-level) and its constituents (micro-level). The internal stability failure of the meso-level is characterized by local bending of the fibres within one or more than one reinforcement systems. It may show itself in certain medium areas. In the cases when defining the internal stability failure is beyond the existing methodologies, the problem can be solved by developing the graphical picture of the phenomenon.

Moreover, visualization seems to be the only means which is able to evidence the internal stability failure on the microlevel of fibre-reinforced material constituents, in particular within the matrix, which is softer. The fact is that this type of the failure is expressed in the form of the matrix folds between the neighbouring reinforcing fibres which may belong to the same or to different systems.

Visualization Methodology for Fibre-Reinforced Materials under Large Deformation

The presented in this paper deformation visualizations of fibre-reinforced material units are developed with the numerical solution of the material boundary problem via two-level Akhundov's carcass theory with input components of microscopic deformation [1, 2]. In its turn, the solution of micro or boundary problem is per the model of a homogeneous body piece. This allows the material inner fields and the material deformed configuration to be defined. They correspond to the macroscopic deformation components, which values are set depending on the monotonically changing parameter of t_s. The latter is related to the overall study of the material deforming and the medium. Their values are defined by the displacement of the frame or salient points of the material unit, in this case the material unit is regarded as a stiff unity. These salient points displacements are the very displacements which enable the specific approach to the boundary problem solution. Moreover, spinning or turning of a deformed unit as a stiff unity is helpful for generating of a quite full deformation picture with 3D imaging.

Furthermore, 3D image of a unit is built with the grit of the nodal points applied to calculate the deformed state. The nodal points on the unit sides act as the control points of the visualization. Their locations in the initial and deformed configurations are connected with interpolation lines. This practice is performed in the full agreement with the logistics of numerical method for a deformed unit and the digitization applied. In deforming the material unit, its flat and quasi-flat faces are locally distorted and fractured on the matrix-fibre boundary due to the difference between the mechanical properties of the unit constituents. This is the reason why the grits of the frame lines intersections on the unit faces are built as two different experiences (one for the matrix area and the other one for the fibre area). The boundary lines between the material constituents are also built apart from the other frame lines, which are drawn being based on the interpolation of Cartesian coordinates x_j^1, x_j^2, x_j^3 (j=0,1,...,n) for the control points located on the unit faces. These frame lines are applied for the line produced by cubic splines $s(t, x^1)$, $s(t, x^2)$, $s(t, x^3)$ in a parametric form [3, 4, 5]. The boundary conditions are set by equality of splines third derivatives on their ends to cubic curves coming through the four first and four last points sets.

The length, which is reckoned along the polygonal line, is used as t parameter of spline interpolation. The polygonal line itself is generated from straight intercepts which connect the control points. Such a practice is motivated by the absence of preliminary information about the curve to pass through control points and is the objective of the curve plotting. The interpolation procedure could be repeated on condition that the length along the curve is regarded as the parameter for the next interpolation. In this case, however, the calculation algorithm for the interpolating curve, which we need to define, is becoming

more complex while its relocalization is not noticeable at the same density of nodal points within the discrete skeleton to be applied for the unit inner fields calculations. Thus, quite reasonable is the parameterization of the cubic splines used for the above-mentioned polygonal line or, named in other words, linear splines, supported by nodal points of the computational scheme for the unit, and the nodal points are treated as the control points of visualization.

The material unit visualization is, in fact, the visualization of the frame lines on the unit sides, it is performed with isometric projections of skew-angle front and those of skew-angle side and diametric rectangular projection [6,7]. The application of several axonometric types is explained by the fact that the linear and angular distortions in the unit 3D imaging are under influence of the unit shapes (both initial one and that after deformation) and its orientation with respect to the image plane. The unit imaging in some projections could be highly distorted and some locally bent or distorted faces of the deformed unit can overlap the other unit parts.

In this case, employment of the different projections is to be more reliable because it enables some parts of the unit boundary surface to be visible or be overlapped to the less extent and this practice does not require changing the distorted unit location with respect to the plane of visualization.

Additionally, we would like to mention that for the work reported we have chosen a computer system with a suitable graphical interface for this kind of work. MATLAB has proved to be such visualization medium. We input in this system the data on material nodal points positions with regard to the calculations for its deformed state [8].

Visualization for Unidirectional Fibre-Reinforced Material

This type of visualization is carried out by the positions of the material unit control points, which have been calculated with Akhundov's carcass theory. The calculation method applied for unidirectional fibre-reinforced material under conditions of large deformations and the results achieved have been reported [9].

Fig. 1 illustrates the configurations of unidirectional fibre-reinforced material with quadrangular fibres in both the initial and deformed states. The configuration images of the unit are given in skew-angle front isometry. The unit is described by the values of the longer side of a rectangular arrangement $a_f = 1.2$ mm, those of the shorter side $b_f = 1$ mm and fibre diameter $d_f = 0.7$ mm. The data given below are to show in details the simulation practice. The material reinforcement ratio is $k_f = \left(\pi d_f^2/4\right)/\left(a_f b_f\right) = 0.3207$. Matrix deformation behavior in this case is simulated with Levinson and Burgess three-constant potential [10].

$$W_m = \frac{E_m}{4\left(1+\nu_m\right)}\left[\beta_m\left(I_1-3\right)+\left(1-\beta_m\right)\left(I_2 I_3^{-1}-3\right)+2\left(1-2\beta_m\right)\left(\sqrt{I_3}-1\right)+\left(2\beta_m+\frac{4\nu_m-1}{1-2\nu_m}\right)\left(\sqrt{I_3}-1\right)^2\right] \quad (1)$$

where E_m = 4MPa, $\nu_m = 0.46$, $\beta_m = 1$ (I_1, I_2, I_3 are tensor invariants of Cauchy and Lagrange strain measure). The reinforcing fibres are simulated with Blatz potential of two constants [11].

$$W_f = \frac{E_f}{4\left(1+\nu_f\right)}\left[\left(I_1-3\right)-\frac{2}{1-2\nu_f}\ln\sqrt{I_3}+\frac{4\nu_f}{1-2\nu_f}\left(\sqrt{I_3}-1\right)\right] \quad (2)$$

where we assume that E_f=1240MPa while $\nu_f = 0.40$ (stiff fibers).

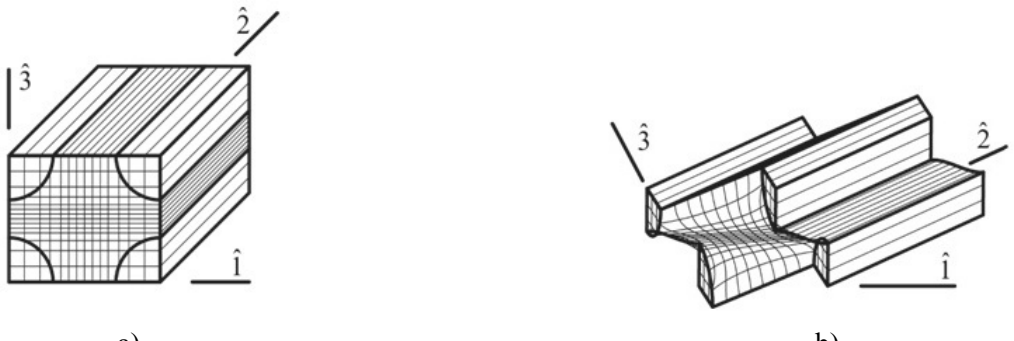

a) b)

Figure 1. Unidirectional Fibre-Reinforced material in its skew-angle front isometry. The configurations of the initial (a) and the deformed (b) states.

For these images, we apply Cartesian rectangular reference system ($\hat{x}^1$) with its axes directed along the unit ribs. The upper level of Akhundov's carcass theory employs the macroscopic version of this reference system, which serves as a means of parameter setting for reinforced material macroscopic deformation, the lower level of the mentioned theory uses the material version of the coordinates for calculating the inner fields. The unit boundary problem is solved with method of local variations [12, 13] and the deadlock conditions of the method are avoided in the appropriate way [14]. The solution is implemented as the result of finite-element grid method with approximation means of isometric finite elements [15, 16].

The unit macroscopic deformation is described with the values of $\hat{\lambda}_i$ and $\hat{\omega}_i$, which are macroscopic elongation ratios along ($\hat{x}^i$) coordinate lines and angles between ($\hat{x}^i$ and $\hat{x}^j$). $\hat{x}^i$ and $\hat{x}^j$ are coordinate lines in its macroscopically deformed configuration. We have defined the unit deformed configuration with the following parameter values: $\hat{\lambda}_1 = 0.85$, $\hat{\lambda}_2 = 1.04$ $\hat{\lambda}_3 = 1.07$, $\hat{\omega}_{12} = 50^o$, $\hat{\omega}_{13} = 100^o$, $\hat{\omega}_{23} = 110^o$.

In the course of the visualization, the deformed unit is located with respect to the non-deformed one in a way to allow the plane of macroscopic axes $\hat{x}^1$ and $\hat{x}^2$ to sustain its orientation when deformation. At this, axis $\hat{x}^1$ has its initial direction. The directions of $\hat{x}^1,...,\hat{x}^3$ axes in the material unit initial and deformed configurations are shown as $\hat{1},...,\hat{3}$ respectively in figure 1 and in the following figures. The control points (15×15) are taken for the visualization, they belong to that unit face which is transverse to the fibre directions and are among the nodal points of the numerical solution for the deformation problem. It is important to note that under deformation, all the faces of the material unit are subjected to the fractures on the matrix-fibre boundary due to the macroscopic shears. Their parts are distorted within the limits of the each material constituent, especially it is noticeable on the matrix front face.

Visualization for the Two-Way Fibre-Reinforced Material

For this visualization, we utilize the earlier developments of the numerical solution for two-way fibre-reinforced material under large deformations and the calculations for this solution [17]. Relying on mentioned paper results, we produce images of a two-way fibre-reinforced material unit in its initial and deformed configurations which are shown as horizontal skew-angle front isometry (see fig. 2). The material specific character is described below.

The matrix is reinforced with the fibres which can be classified as two families by their direction. When the material is in the initial state, the structural macroelement of the unit is characterized by the angle ($\gamma_f = 31°$) between fibre directions or fibres belonging to the different families. The fibres of the both reinforced families have the same distances between their centerlines: within one reinforcement plane ($a_f = 1.3$ mm) and between the parallel planes ($b_f = 2$ mm). The fibre diameter of the both families is $d_f = 0.7$ mm . In this reinforcement geometry, the material stuffed with the fibres, is illustrated by $k_f = \left(2\cdot\pi d_f^2/4\right)/\left(a_f b_f\right) = 0.296$. The matrix material is simulated with potential (1), where the constants values are E_m = 4 MPa,ν_m = 0.46, β_m = 1, while the simulation of the fibres is performed with potential (2), where the constants values are E_f = =1240 MPa, ν_m = 0.40 (stiff fibres).

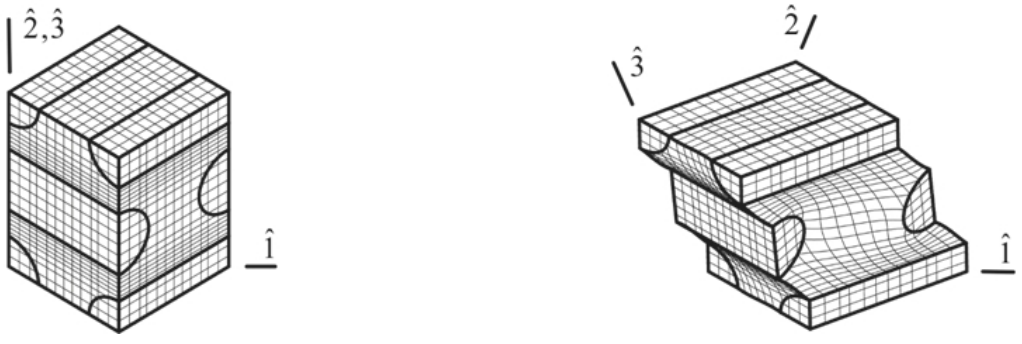

a) b)

Figure 2. The images of two-way fibre-reinforced material in horizontal skew-angle front isometry. Its initial (a) and deformed (b) configurations

The Cartesian rectangular reference system $\hat{x}^i$ acts as the basic coordinates related to the material units and is applied for macroscopic deformation setting. The axes of $\hat{x}^1$ and $\hat{x}^2$ are directed per the

rhombus diagonals of the two-way scheme for the non-deformed unit, axes $\hat{x}^3$ – per its height. In the figure, you may see these axes marked as $\hat{1}$, ..., $\hat{3}$ respectively. The calculations for the unit configuration with the given parameters of its macroscopic deformation are carried out with the oblique axes of Cartesian reference system. The latter is determined by the directions of two-way fibres centerlines. The visualization employs 13×25, 13×25, 13×13 control points within the front, side and horizontal faces of the unit and the control points are taken from the scheme of the numerical solution for deforming.

The macroscopic deformation parameters to serve for the calculations of the unit configurations are as follows: $\hat{\lambda}_1 = 1.18$, $\hat{\lambda}_2 = 0.97$, $\hat{\lambda}_3 = 1.06$, $\hat{\omega}_{12} = 64^o$, $\hat{\omega}_{13} = 112^o$, $\hat{\omega}_{23} = 104^o$ We observe that the centerlines of one-family fibres are elongated significantly while those directed to the other way are shortened; the distances and angles between them within the reinforcement plane also show the changes. However, neither the parameters of the deformed geometry nor the deformation parameters ($\hat{\lambda}_1$, $\hat{\lambda}_2$, $\hat{\omega}_{12}$) are distorted in the projection applied. Therefore, they can be measured within the image due to the orientation of the unit, which is assumed as a stiff entity, referred to the image plane. The other important condition is that the corresponding dimensions of the initial unit image are assumed as the scale values in linear deformations.

Visualization of Tri-Orthogonally Fibre-Reinforced Material

Figures 3 – 5 illustrate the material unit of tri-orthogonal fibre-reinforcement system in the initial state and in the state under deformation. The deformed configuration has been calculated per the model earlier developed and submitted in [18]. The material unit is relevant to the coordinate system $\hat{x}^i$, which axes are directed along the unit ribs. To show the initial and deformed states of the material unit, we apply macroscopic locations of the axes as straight lines passing through the cube corners.

In the initial state, the material unit is a cube. The reinforcement ratio for the each reinforcement system is $k_{fi} = 0.1$ at total fibre embedment of $k_f = k_{f1} + k_{f2} + k_{f3} = 0.3$. Similarly, the fibre diameters of the reinforcement system are $d_{fi} = \sqrt{4 \cdot k_{fi} / \pi} = 0.3568$ mm, the distance or step between the fibre center lines in the reinforcement system is $a_f = b_f = c_f = 1$mm. The material of the matrix is simulated by means of potential (1) with constants of $E_m = 4$ MPa, $\nu_m = 0.40$, and $\beta_m = 1$, while the material of the fibres is described as potential (2) with constants of $E_f = 68$ MPa and $\nu_f = 0.40$, (softer fibres).

According to the technique applied to this types of materials, the deformed unit in this case is also located respectively to the same non-deformed material in a way to have the plane of macroscopic axes ($\hat{x}^1$ and $\hat{x}^2$) unchangeable under deformation in terms of its orientation. Axis $\hat{x}^1$ remains in its initial direction.

The unit macroscopic deformation, which determines the material configuration, is set by the following parameters: $\hat{\lambda}_1 = \hat{\lambda}_3 = 1.22$, $\hat{\lambda}_2 = 1.49$, $\hat{\omega}_{12} = 46^o$, $\hat{\omega}_{13} = 120^o$, $\hat{\omega}_{23} = 134^o$ .The solution for the microboundary problem for the material unit as well as those of uni-directional and two-way fibre-reinforced ones is generated with application of isoparametric finite element. The material configuration visualization is performed with control points of 19×25, 19×25, 19×19, located at the unit faces and taken from the nodal points of the numerical solution for the deformation.

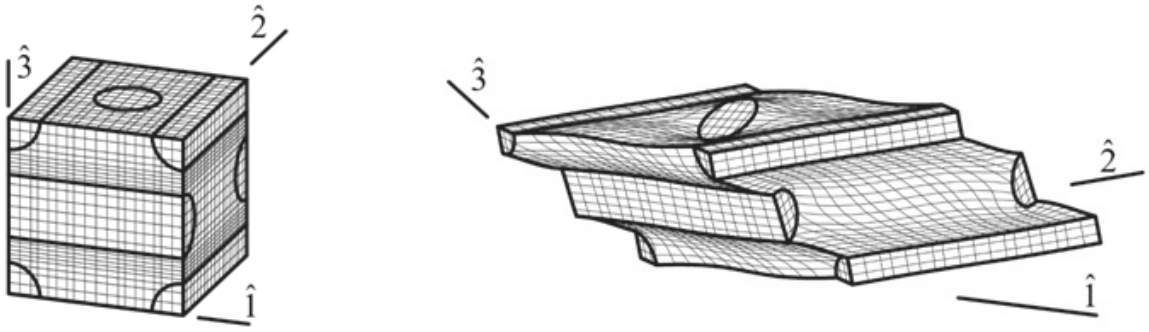

a) b)

Figure 3. The images of tri-orthogonally fibre-reinforced material in orthographic dimetric projection. The initial state (a) and the state under deformation (b), regarded as reference positions

The orthographic dimetric projection in figure 3 is defined by the location of those axes which are related with the non-deformed unit axes ($\hat{x}^i$) with respect to the projections plane.

Commenting on figure 4, we would like to specify that in order to watch the material unit from the back side, we turned it 180 degrees round axis $\hat{x}^3$ with respect to the reference position.

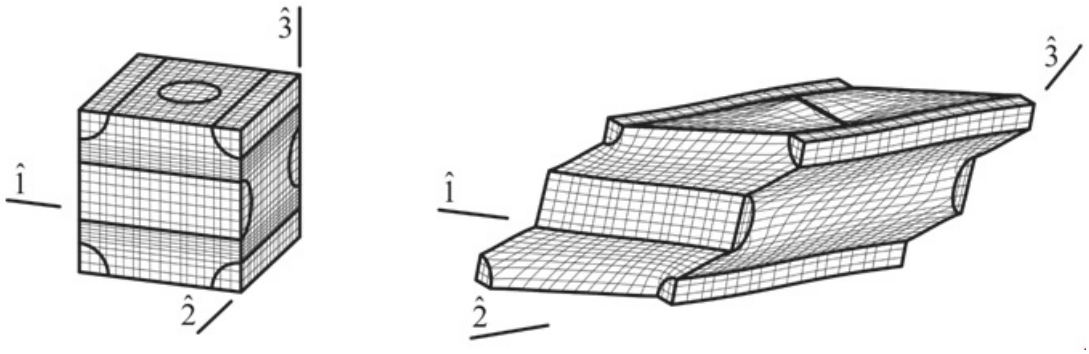

a) b)

Figure 4. The same tri-orthogonally fibre-reinforced material when 180 degrees turn of the material unit round axis $\hat{x}^3$

Moreover, if we turn both the material unit in the initial form (3a) and that in the deformed configuration (3b) as far as 270 degrees round axis $\hat{x}^3$, we obtain the another view (see fig. 5) of the material unit, in the initial form (a) and under deformation (b) respectively.

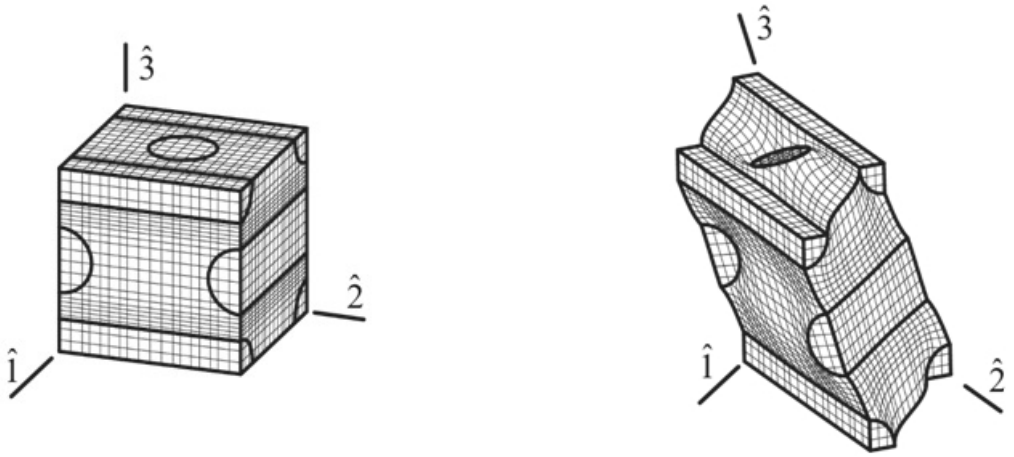

a) b)

Figure 5. The same tri-orthogonally fibre-reinforced material when 270 degrees turn of the material unit round axis $\hat{x}^3$

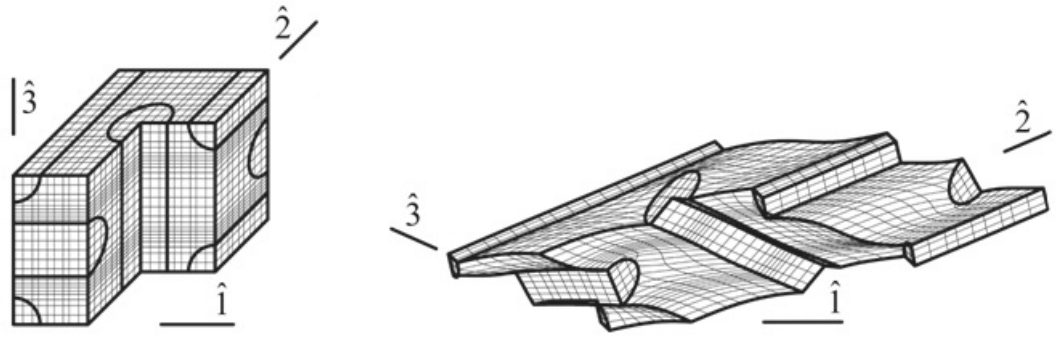

a) b)

Figure 6. The images of tri-orthogonally fibre-reinforced material with the cut of its front quarter from the right in skew-angle front isometry. The initial configuration (a) and the configuration under deformation (b)

Let us concentrate our attention on the considerable spatial distortions of the fibre centerlines and other longitudinal material lines. The fibre in the very centre changes its orientation noticeably due to vast transversal shears in the material.

Furthermore, figures 6a and 6b are produced to show the behaviour of the material unit, which has the cut of its front quarter from the right. These images are made in skew-angle front isometry and are able to reveal the specific character of the deformed central fibre.

Conclusions

The methodology to visualize fibre-reinforced materials under large deformations is applicable for the units with unidirectional, bidirectional and three-directional schemes of reinforcement. This visualization reflects the quality of the material inner fields and to a certain extent describes them numerically therefore there are prerequisites to regard it as an effective means of material representations in the deformed state. With application of the developed practice, one can perform visualization of a reinforced material behaviour under deformation relying on the calculations of medium inner fields at the steps of the loading events.

References:

1. Akhundov V. M. (1998) Structural macroscopic theory of stiff and soft composites. Invariant description. *Mechanics of Composite Mate- rials*. Vol. 34, No. 5. p.p. 419-432.
2. Akhundov V. M. (2000) Carcass theory of fibrous media with incurved and locally curved fibers as large deformations. *Mechanics of Composite Materials*. Vol. 6, No. 6. p.p. 275–293.
3. Zav'yalov Yu.S. (1985) *Splayny v inzhenernoy geometrii* [Splines in engineering geometry]. Moscow: Mashinostroenie. 224 p.
4. Shup T. (1982) *Reshenie inzhenernykh zadach na EVM* [Computer assisted engineering problems solutions]. Moscow: Mir. 238 p.
5. Forsythe G.E. Malcolm M.A., Moler C.B. (1977) *Computer Methods for Mathematical Computations*. Englewood Cliffs, N.J. Prentice-Hall. 270 p.
6. Mikhaylenko V.E. (1990) *Inzhenernaya grafika* [Engineering graphics]. Kiev: Vishcha shk. 303 p.
7. Mc Reynolds T., Blythe. D (2005) *Advanced graphics programming using openGL*. Elsevier. 502 p.
8. D'yakonov V.P. (2008) *MATLAB7.*/R2006/ R2007: Samouchitel'* [MATLAB7.*/R2006/ R2007: Guide]. Moscow: DMK Press. 768 p.
9. A Akhundov V. M. (1999) Analysis of elastomeric composites based on fiber-reinforced systems. Unidirectional composites. *Mecha- nics of Composite Materials*. Vol. 35. No. 1. – p. p. 19-32.
10. Levinson M. and Burgess I. W. (1971) A comparison of some simple constitutive relations for slightly compressible rubber-like materials. *Int. J. Mech. Sci*. Vol. 13. p. p. 563—572.
11. Blatz P. J. (1960) Application of finite elastic theory in predicting the performance of solid propellant rocket motors. *Calif. Inst. of Techn. GALCJISM*. p. p. 60—125.
12. Chernous'ko F.L. (1973) *Variatsionnye zadachi mekhaniki i upravleniya* [Variational problems of mechanics and control]. Moscow: Nauka. 238 p.
13. Vasil'ev F.P. (2002) *Metody optimizatsii* [Optimization methods]. Moscow: Factorial Press. 824 p.
14. Fedorenko R.P. (1978) *Priblizhennoe reshenie zadach optimal'nogo upravleniya* [Approximate solution for the optimal control problrms]. Moscow: Nauka. 448 p.
15. Sakharov A.S., Al'tenbakh I. *Metod konechnykh elementov v mekhanike tverdykh tel* [Finite elements method in solid bodies mechanics]. Kiev: Vishcha shkola. 480 p.
16. Zenkevich O., Morgan K. (1986) *Konechnye elementy i approksimatsiya* [Finite elements and approximation]. Moscow: Mir. 318 p.
17. Akhundov V. M. (1999) Analysis of elastomeric composites based on fiber-reinforced systems. 3. Two-directional composites. *Mechanics of Composite Materials*. Vol. 35, No. 4. p.p.325-334.
18. Akhundov V. (2001) M. Analysis of elastomeric composites based on fiber-reinforced systems. 4. 3D Composites. *Mechanics of Composite Materials*. Vol. 37, No. 3. p.p. 223-236.